In Silico Prediction of Inhibitory Potential of a Punicalagin β-anomer Against SARS-COV-2 Main Protease (Mpro)

Norberto Monteiro (norbertokv@ufc.br)
Federal University of Ceara: Universidade Federal do Ceara https://orcid.org/0000-0002-5847-5733
Vitória Monteiro
Centro Universitário Christus: Centro Universitario Christus
Lorena Lima
Centro Universitário Christus: Centro Universitario Christus
Anna Karolline
Centro Universitário Christus: Centro Universitario Christus
Richele Machado
Centro Universitário Christus: Centro Universitario Christus

Research Article

Keywords: molecular docking, molecular dynamics, Coronavirus. Punica granatum, Pomegranate, SARS-CoV-2.

Posted Date: September 20th, 2021

DOI: https://doi.org/10.21203/rs.3.rs-672767/v1

Abstract

The pandemic caused by the new coronavirus has resulted in a global health emergency and has prompted an urgent need for new treatment strategies. No target-specific drugs are currently available for SARS-CoV-2, but new drug candidates targeting the viral replication cycle are being explored. A prime target of drug-discovery efforts is the SARS-CoV-2 main protease (Mpro). In this work, we identified a potential inhibitor for SARS-CoV-2 main protease using *in silico* methodologies. Molecular docking and molecular dynamics studies were carried out to ascertain the inhibitory action of α and β anomers of Punicalagin from fruit peel of *Punica granatum* against the Mpro protease. The molecular dynamics results revealed that the β-anomeric configuration of punicalagin allowed access to more hydrogen bonds and hydrophobic interaction leading to higher selectivity and specificity of β-anomer than α-anomer. Therefore, the β-anomer of Punicalagin could act as potential inhibitor against the main protease of SARS-CoV-2 and may act as a potential drug candidate.

Introduction

The outbreak caused by a new species of coronavirus led the World Health Organization (WHO) in early 2020 to declare the disease caused by this virus as a Public Health Emergency of International Importance and soon after it was characterized as a pandemic[1]. In December 2019, in the city of Wuhan, China, an outbreak occurred, in which several individuals went to local hospitals with severe pneumonia of unknown etiology. After investigations to find out about the cause of this outbreak, it was found that most of the initial cases had contact with the same wholesale seafood market[2]. The etiologic agent discovered was a new virus of the family Coronaviridae and genus β-coronavirus and was identified as severe acute respiratory syndrome of coronavirus 2 (SARS-CoV-2), which causes coronavirus 2019 or COVID-19, as it became known. In addition, it was shown that, unlike other coronaviruses that infect humans, SARS-CoV-2 has a high human-to-human transmission rate, which was a determining factor for its dissemination[3, 4].

The virus can infect individuals of all ages, however it mainly affects men over 60 years[5]. According to He, Deng and Li[6], the lethality rate is higher in patients with coexisting medical conditions, such as diabetes, hypertension and cardiovascular diseases. Symptoms vary from fever, cough, sore throat, changes in smell and taste to acute respiratory distress syndrome (ARDS) and dyspnoea in the most severe cases[6–8].

The SARS-CoV-2 virus consists of four structures, the spike glycoprotein or S glycoprotein, a membrane protein, an envelope protein and a nucleocapsid protein, which is present within the viral envelope[9]. SARS-CoV-2 is a ribonucleic acid (RNA) virus whose genetic material is a single positive RNA molecule. The virus enters the human host, through the binding of the spike glycoprotein, in the S1 subunit, with its receptor, the angiotensin-converting enzyme 2 (ACE2) that is present on the cell surface[10]. After binding, Furin enzyme will pre-cleave the S glycoprotein in the S1 and S2 subunits and then the transmembrane serine protease 2 (TMPRSS2) enzyme will cleave the S glycoprotein in the S2 subunit. Subsequently, the

S2 subunit will assist in the fusion of the viral membrane with the host cell membrane and thus, with the entry of the virus into the host cell[4, 11].

The SARS-CoV-2 main protease is an enzyme called Mpro or 3C-like protease (3CLpro), that plays an important role in the replication cycle, thus becoming a potential target for the control of viral infection[12]. Its action occurs after the virus enters the host cells, where the viral RNA genome will translate inactive proteins, called pp1a and pp1ab, which will be cleaved through Mpro and will result in non-structural proteins and join the RNA to form the virus genome[13]. Thus, it becomes necessary means for inhibiting replication of the SARS-CoV-2 virus. Researchers are seeking out products with efficient antiviral activity to prevent the SARS-CoV-2 virus replication. The peel of pomegranate (*Punica granatum*), has substantial studies that encompass antibacterial[14], anti-inflammatory[15] and antioxidant[16] activities in addition to antiviral activity agaist Influenza virus[17], Human Immunodeficiency virus (HIV)[18] and Herpes simplex virus[19]. Punicalagin is a phenolic compound present abundantly in pomegranate peel with high molecular weight[20]. Punicalagin is found naturally in two anomeric forms α and β differing from the chiral carbon position (Fig. 1). Recent studies including α/β anomers[21–23] revels that there are differences in the non-covalent interactions profile between these anomers and proteins.

Hence, the present *in silico* study was aimed to explore the differences in inhibitory potential of α/β anomers of Punicalagin against the main protease viral of SARS-CoV-2 (Mpro).

Computational Details

Preparation of Mpro and α/β anomers

The protonation states of the molecules has a significant influence on its mode of interaction with the receptor. Based on the pKa values, the protonation states of the α/β anomers studied were calculated using the ChemAxon's MARVIN software[24].

The geometries of the α/β anomers were optimized by using standard techniques[25]. Optimization calculations were performed by using Density Functional Theory[26] (DFT) method at B3LYP functional[27] along with 6–31 + G(d,p) basis set implemented in Gaussian 16 package[28]. Vibrational modes of the optimized geometries were calculated in order to determine whether the resulting geometries are true minima or transition states. All optimization calculations were performed in solution by using Polarizable Continuum Model (PCM)[29] with the Integral Equation Formalism (IEF)[30] using water as a solvent. The optimized structures with the lowest energy were used for the molecular docking calculations.

The X ray crystal structure of COVID-19 main protease (Mpro) in complex with an inhibitor N3[31] at 2.16 Å resolution (PDB ID: 6LU7) used is this study was obtained from RCSB Protein Data Bank[32]. The Mpro structure was prepared for molecular docking by removing the water molecules and other hetero molecules from the original crystal structure.

The molecular docking study

Docking Input files were created using AutoDock tools of MGL tools[33, 34]. The 3D grid box with a box size of 30 Å x 30 Å x 30 Å with the center coordinates x = -13.579, y = 18.940 and z = 69.318, which are the coordinates in the Nε2 of His41 residue that is included in the Mpro catalytic dyad[35]. Molecular docking was performed using Autodock Vina[36]. Nine best poses were generated for each anomer and scored using Autodock Vina scoring functions. The lowest energy pose of each anomer was used as input for molecular dynamics (DM) simulations.

Molecular dynamics simulations

All molecular dynamics (MD) simulations were performed using the GROMACS 2018.4[37] package implemented with the AMBER ff99SB[38]. The transferable intramolecular potential with 3 points (TIP3P) [39] water molecules were used to solvate the simulated systems. The systems neutralization was achieved through the addition of counter ions. The Leap-Frog algorithm[40] was applied to integrate the motion equation with time step of 2.0 fs. The long-range interactions were modeled using particle-mesh Ewald sum (PME)[41] with a cut-off of 1.2 nm. The van der Waals interactions were also calculated using the same threshold. Bonds involving hydrogen atoms were restrained using LINCS algorithm[42]. The Nosé–Hoover thermostat[43] was used to fix the system temperature (310 K) in all production simulations, while the system pressure was controlled using a Parrinello–Rahman barostat[44] in the NPT simulations. The geometry of the systems were minimized by the steepest descent algorithm[45] for 10000 steps with tolerance of 10 kJ mol^{-1} nm^{-1} followed by conjugate gradient algorithm[46] for 10000 steps with tolerance of 10 kJ mol^{-1} nm^{-1}. Two shorts 20-ns equilibrium dynamics with NVT and NPT ensembles were performed. Finally, 200-ns production MD simulation using NVT ensemble was performed in three replicates for each system in order to determine the interaction energy between α/β anomers and Mpro.

To analyze the interaction energy between α/β anomers and Mpro we used the Interaction Potential Energy (*IPE*)[47], which can be defined as the total interaction energy between two groups, α/β anomers and Mpro. The *IPE* calculation includes the sum of van der Waals and electrostatic contributions. To identify non-covalent interactions between anomers and Mpro receptor, we used an open-source protein–ligand interaction profiler (PLIP)[48]. The graphical representations of the protein-receptor interaction were built with Visual Molecular Dynamics (VMD)[49] software from PLIP analysis.

Results And Discussion

The *p*Ka can predict the protonation states of organic molecules across *pH* range. Ionizable sites are found often in organic molecules and influence their pharmaceutical properties including target affinity[50]. Due to the importance of knowing the protonation state, the microspecies distribution (%) as a function of *pH* (1.0–14.0) for α/β anomers were performed (Supplementary Fig. S1). The *p*Ka values of hydroxyl groups are shown in the Supplementary Figs. S2a (α anomer) and S2b (β anomer). We can see

that the *p*Ka values do not change with configuration change and then α/β anomers have the same ionizable sites at pH = 7.4, that are indicated by blue arrows in Supplementary Fig. S2a. Hence, negatively charged punicalagin α/β anomers were considered for this study. In order to improve the structures of α/β anomers their optimized structures were performed by Density Functional Theory (DFT) using B3LYP/6–31 + G(d,p) level of theory (Fig. 2).

From α and β optimized structures and using Mpro as receptor, the best poses (pose 1) generated from docking analysis (Supplementary Fig. S3), MD simulations were performed for identifying the α/β anomers intermolecular interaction profile. The interaction potential energy (*IPE*) calculations were performed to evaluate the affinity as well as the contribution of each residue of binding pocket of Mpro receptor with the ligands. Based on atoms of α/β anomers as reference, the RMSD analysis (Fig. 3) showed a structural equilibrium around 125 ns for α (Fig. 3A, black, red and green lines) and around 50 ns for β (Fig. 3B, blue, orange and purple lines). Thus, the *IPE* calculations were performed in the last 75 ns for α anomer and 150 ns for the β anomer. The average *IPE* (standard deviation) between Mpro receptor and α/β anomers were − 250.96 kJ mol^{-1} (20.40) and − 320.00 kJ mol^{-1} (27.05), respectively. Then, according to the *IPE* values, β anomer has a highest affinity for Mpro compared to the α anomer. This result suggests that the β anomer can become a potential inhibitor for SARS-CoV-2 main protease.

A closed comparative analysis of the binding of α (Fig. 4a) and β (Fig. 4b) anomers with pocket Mpro residues in the last simulation frame (200 ns) of MD, revealed that the β anomer binds to the protein through nine favorable hydrogen bonds. On the other hand, a close inspection of the binding of α anomer (Fig. 4a) with pocket Mpro residues showed that α anomer ligand binds with the protein with seven hydrogen bonds. Hydrogen bonds contribute from 11 to 60 kJ mol^{-1} in the interaction potential energy (*IPE*)[51] and are force intermolecular most influential in molecular recognition[52]. Furthermore, the β-anomeric carbon configuration (Fig. 5) allowed the holding of two hydrogen bonds (blue dashed line) and one hydrophobic interaction (gray dashed line) with THR45 Mpro residue. We can see in Fig. 5 that two hydrogen bonds are formed between hydroxyl groups of β-anomeric carbon and residue THR45 at distances of 3.42 Å and 4.74 Å. In addition, the hydrophobic interaction is formed between C-γ of residue THR45 and C-47 of β anomer. The presence of hydrophobic groups in the ligand can expel molecular water from protein pocket and maximize hydrogen bonds account leading to an increased selectivity and efficiency of the receptor for a certain ligand[53], as in the case of the β-anomer and Mpro receptor, where the β-anomeric configuration of punicalagin allowed access to two more hydrogen bonds and a hydrophobic interaction. In other words, the combination of hydrogen bonds and hydrophobic interaction found between β-anomer and Mpro binding pocket led to higher selectivity and specificity of the β-anomer ligand compared to the α-anomer.

Conclusion

In this work, we reported a systematic study of affinity and specificity of α- and β- anomers of Punicalagin with Mpro protease of SARS-CoV-2 by using molecular docking and molecular dynamics simulations. Interaction Potential Energy (*IPE*) calculations through molecular dynamics simulations reveals that the

β-anomer of Punicalagin has a higher affinity for the pocket Mpro receptor compared to the α-anomer. Furthermore, β-anomer configuration shows more hydrogen bonds and a hydrophobic interaction than α-anomer with pocket Mpro residues. The amount and combination of hydrogen bonds and hydrophobic interaction can lead to selectivity and specificity of β-anomer of Punicalagin being able to act as a potential drug candidate. Therefore, we way conclude that the β-anomer ligand could act as potential inhibitor against the main protease of SARS-CoV-2.

Declarations

Supplementary data

The online version contains supplementary material available at

Author contributions

Vitória Monteiro, Lorena Lima, Anna Karolline and Richele Machado: Contribution to the writing and revising of the manuscript. Norberto Monteiro: Contribution to the theoretical calculations and to the writing and revising of the manuscript.

Code availability

Not applicable.

Data Availability

All data are available on request to the corresponding author.

Conflict of interest

The authors declares no competing interests.

Acknowledgements

The authors thank High-Performance Computing Center (NPAD) at Federal University of Rio Grande do Norte (UFRN) and the National High-Performance Processing Center of the Federal University of Ceará (UFC) for providing computational resources.

References

1. Zoumpourlis V, Goulielmaki M, Rizos E, et al (2020) The COVID-19 pandemic as a scientific and social challenge in the 21st century. Mol Med Rep 22:3035–3048. https://doi.org/10.3892/mmr.2020.11393
2. Singhal T (2020) A Review of Coronavirus Disease-2019 (COVID-19). Indian J Pediatr 87:281–286. https://doi.org/10.1007/s12098-020-03263-6

3. Salazar E, Perez KK, Ashraf M, et al (2020) Treatment of Coronavirus Disease 2019 (COVID-19) Patients with Convalescent Plasma. Am J Pathol 190:1680–1690. https://doi.org/10.1016/j.ajpath.2020.05.014
4. Suručić R, Tubić B, Stojiljković MP, et al (2021) Computational study of pomegranate peel extract polyphenols as potential inhibitors of SARS-CoV-2 virus internalization. Mol Cell Biochem 476:1179–1193. https://doi.org/10.1007/s11010-020-03981-7
5. Guan W, Ni Z, Hu Y, et al (2020) Clinical Characteristics of Coronavirus Disease 2019 in China. N Engl J Med 382:1708–1720. https://doi.org/10.1056/NEJMoa2002032
6. He F, Deng Y, Li W (2020) Coronavirus disease 2019: What we know? J Med Virol 92:719–725. https://doi.org/10.1002/jmv.25766
7. Berlin DA, Gulick RM, Martinez FJ (2020) Severe Covid-19. N Engl J Med 383:2451–2460. https://doi.org/10.1056/NEJMcp2009575
8. Giacomelli A, Pezzati L, Conti F, et al (2020) Self-reported Olfactory and Taste Disorders in Patients With Severe Acute Respiratory Coronavirus 2 Infection: A Cross-sectional Study. Clin Infect Dis 71:889–890. https://doi.org/10.1093/cid/ciaa330
9. Senger MR, Evangelista TCS, Dantas RF, et al (2020) COVID-19: molecular targets, drug repurposing and new avenues for drug discovery. Mem Inst Oswaldo Cruz 115:1–32. https://doi.org/10.1590/0074-02760200254
10. Shang J, Wan Y, Luo C, et al (2020) Cell entry mechanisms of SARS-CoV-2. Proc Natl Acad Sci U S A 117:11727–11734. https://doi.org/10.1073/pnas.2003138117
11. Zhou M, Zhang X, Qu J (2020) Coronavirus disease 2019 (COVID-19): a clinical update. Front Med 14:126–135. https://doi.org/10.1007/s11684-020-0767-8
12. Jin Z, Du X, Xu Y, et al (2020) Structure of Mpro from SARS-CoV-2 and discovery of its inhibitors. Nature 582:289–293. https://doi.org/10.1038/s41586-020-2223-y
13. Zhang R, Li Y, Zhang AL, et al (2020) Identifying airborne transmission as the dominant route for the spread of COVID-19. Proc Natl Acad Sci 117:14857–14863. https://doi.org/10.1073/pnas.2009637117
14. Voravuthikunchai SP, Sririrak T, Limsuwan S, et al (2005) Inhibitory Effects of Active Compounds from Punica granatum Pericarp on Verocytotoxin Production by Enterohemorrhagic Escherichia coli O157 : H7. J Heal Sci 51:590–596. https://doi.org/10.1248/jhs.51.590
15. Colombo E, Sangiovanni E, Dell'Agli M (2013) A Review on the Anti-Inflammatory Activity of Pomegranate in the Gastrointestinal Tract. Evidence-Based Complement Altern Med 2013:1–11. https://doi.org/10.1155/2013/247145
16. Oudane B, Boudemagh D, Bounekhel M, et al (2018) Isolation, characterization, antioxidant activity, and protein-precipitating capacity of the hydrolyzable tannin punicalagin from pomegranate yellow peel (Punica granatum). J Mol Struct 1156:390–396. https://doi.org/10.1016/j.molstruc.2017.11.129

17. Moradi MT, Karimi A, Shahrani M, et al (2019) Anti-influenza virus activity and phenolic content of pomegranate (punica granatum l.) peel extract and fractions. Avicenna J Med Biotechnol 11:285–291
18. Shaygannia E, Bahmani M, Zamanzad B, Rafieian-Kopaei M (2016) A Review Study on Punica granatum L. J Evidence-Based Complement Altern Med 21:221–227. https://doi.org/10.1177/2156587215598039
19. Arunkumar J, Rajarajan S (2018) Study on antiviral activities, drug-likeness and molecular docking of bioactive compounds of Punica granatum L. to Herpes simplex virus - 2 (HSV-2). Microb Pathog 118:301–309. https://doi.org/10.1016/j.micpath.2018.03.052
20. Gil MI, Tomás-Barberán FA, Hess-Pierce B, et al (2000) Antioxidant Activity of Pomegranate Juice and Its Relationship with Phenolic Composition and Processing. J Agric Food Chem 48:4581–4589. https://doi.org/10.1021/jf000404a
21. Saparbaev E, Aladinskaia V, Yamaletdinov R, et al (2020) Revealing Single-Bond Anomeric Selectivity in Carbohydrate–Protein Interactions. J Phys Chem Lett 11:3327–3331. https://doi.org/10.1021/acs.jpclett.0c00871
22. Rozada T, de Melo U, Pontes R, et al (2018) Facial Selectivity between Carbohydrates and Aromatic Amino Acids Explained by a Combination of NCI, NBO and EDA Techniques with NMR Spectroscopy. J Braz Chem Soc 30:948–967. https://doi.org/10.21577/0103-5053.20180241
23. Mazik M, Radunz W, Sicking W (2002) High α/β-Anomer Selectivity in Molecular Recognition of Carbohydrates by Artificial Receptors. Org Lett 4:4579–4582. https://doi.org/10.1021/ol0201759
24. ChemAxon (2020) Marvin | ChemAxon. https://chemaxon.com/products/marvin. Accessed 13 Mar 2021
25. Chambers LG, Fletcher R (2001) Practical Methods of Optimization. Math Gaz 85:562. https://doi.org/10.2307/3621816
26. Zinola CF (2010) Electrocatalysis: Computational, Experimental, and Industrial Aspects. CRC Press
27. Perdew JP, Burke K, Ernzerhof M (1996) Generalized Gradient Approximation Made Simple. Phys Rev Lett 77:3865–3868. https://doi.org/10.1103/PhysRevLett.77.3865
28. Frisch MJ, Trucks GW, Schlegel HE, et al (2016) Gaussian 16. Gaussian, Inc., Wallingford CT,
29. Mennucci B (2012) Polarizable continuum model. Wiley Interdiscip Rev Comput Mol Sci 2:386–404. https://doi.org/10.1002/wcms.1086
30. Mennucci B, Cancès E, Tomasi J (1997) Evaluation of Solvent Effects in Isotropic and Anisotropic Dielectrics and in Ionic Solutions with a Unified Integral Equation Method: Theoretical Bases, Computational Implementation, and Numerical Applications. J Phys Chem B 101:10506–10517. https://doi.org/10.1021/jp971959k
31. Jin Z, Du X, Xu Y, et al (2020) Structure of Mpro from SARS-CoV-2 and discovery of its inhibitors. Nature 582:289–293. https://doi.org/10.1038/s41586-020-2223-y

32. Berman HM, Battistuz T, Bhat TN, et al (2002) The protein data bank. Acta Crystallogr Sect D Biol Crystallogr 58:899–907. https://doi.org/10.1107/S0907444902003451
33. Holt PA, Chaires JB, Trent JO (2008) Molecular docking of intercalators and groove-binders to nucleic adds using autodock and surflex. J Chem Inf Model 48:1602–1615. https://doi.org/10.1021/ci800063v
34. Morris GM, Ruth H, Lindstrom W, et al (2009) Software news and updates AutoDock4 and AutoDockTools4: Automated docking with selective receptor flexibility. J Comput Chem 30:2785–2791. https://doi.org/10.1002/jcc.21256
35. Chhetri A, Chettri S, Rai P, et al (2021) Synthesis, characterization and computational study on potential inhibitory action of novel azo imidazole derivatives against COVID-19 main protease (Mpro: 6LU7). J Mol Struct 1225:1–13. https://doi.org/10.1016/j.molstruc.2020.129230
36. Trott O, Olson AJ (2009) AutoDock Vina: Improving the speed and accuracy of docking with a new scoring function, efficient optimization, and multithreading. J Comput Chem 31:1–7. https://doi.org/10.1002/jcc.21334
37. Van Der Spoel D, Lindahl E, Hess B, et al (2005) GROMACS: Fast, flexible, and free. J Comput Chem 26:1701–1718. https://doi.org/10.1002/jcc.20291
38. Lindorff-Larsen K, Piana S, Palmo K, et al (2010) Improved side-chain torsion potentials for the Amber ff99SB protein force field. Proteins Struct Funct Bioinforma 78:1950–1958. https://doi.org/10.1002/prot.22711
39. Jorgensen WL, Chandrasekhar J, Madura JD, et al (1983) Comparison of simple potential functions for simulating liquid water. J Chem Phys 79:926–935. https://doi.org/10.1063/1.445869
40. Van Gunsteren WF, Berendsen HJC (1988) A Leap-frog Algorithm for Stochastic Dynamics. Mol Simul 1:173–185. https://doi.org/10.1080/08927028808080941
41. Darden T, York D, Pedersen L (1993) Particle mesh Ewald: An N ·log(N) method for Ewald sums in large systems. J Chem Phys 98:10089–10092. https://doi.org/10.1063/1.464397
42. Hess B, Bekker H, Berendsen HJC, Fraaije JGEM (1997) LINCS: A linear constraint solver for molecular simulations. J Comput Chem 18:1463–1472. https://doi.org/10.1002/(SICI)1096-987X(199709)18:12<1463::AID-JCC4>3.0.CO,2-H
43. Hoover WG (1985) Canonical dynamics: Equilibrium phase-space distributions. Phys Rev A 31:1695–1697. https://doi.org/10.1103/PhysRevA.31.1695
44. Nosé S, Klein ML (1983) Constant pressure molecular dynamics for molecular systems. Mol Phys 50:1055–1076. https://doi.org/10.1080/00268978300102851
45. Arfken GB, Weber HJ, Harris FE (2013) Mathematical Methods for Physicists. Elsevier
46. Hestenes MR, Stiefel E (1952) Methods of conjugate gradients for solving linear systems. J Res Natl Bur Stand (1934) 49:409. https://doi.org/10.6028/jres.049.044
47. Amorim-Carmo B, Daniele-Silva A, Parente AMS, et al (2019) Potent and Broad-Spectrum Antimicrobial Activity of Analogs from the Scorpion Peptide Stigmurin. Int J Mol Sci 20:623.

https://doi.org/10.3390/ijms20030623

48. Salentin S, Schreiber S, Haupt VJ, et al (2015) PLIP: Fully automated protein-ligand interaction profiler. Nucleic Acids Res 43:W443–W447. https://doi.org/10.1093/nar/gkv315
49. Humphrey W, Dalke A, Schulten K (1996) VMD: Visual molecular dynamics. J Mol Graph 14:33–38. https://doi.org/10.1016/0263-7855(96)00018-5
50. Işık M, Rustenburg AS, Rizzi A, et al (2021) Overview of the SAMPL6 pKa challenge: evaluating small molecule microscopic and macroscopic pKa predictions. J Comput Aided Mol Des 35:131–166. https://doi.org/10.1007/s10822-020-00362-6
51. Pace CN, Fu H, Fryar KL, et al (2014) Contribution of hydrogen bonds to protein stability. Protein Sci 23:652–661. https://doi.org/10.1002/pro.2449
52. Dong J, Davis AP (2021) Molecular Recognition Mediated by Hydrogen Bonding in Aqueous Media. Angew Chemie Int Ed 60:8035–8048. https://doi.org/10.1002/anie.202012315
53. Yao H, Ke H, Zhang X, et al (2018) Molecular Recognition of Hydrophilic Molecules in Water by Combining the Hydrophobic Effect with Hydrogen Bonding. J Am Chem Soc 140:13466–13477. https://doi.org/10.1021/jacs.8b09157

Figures

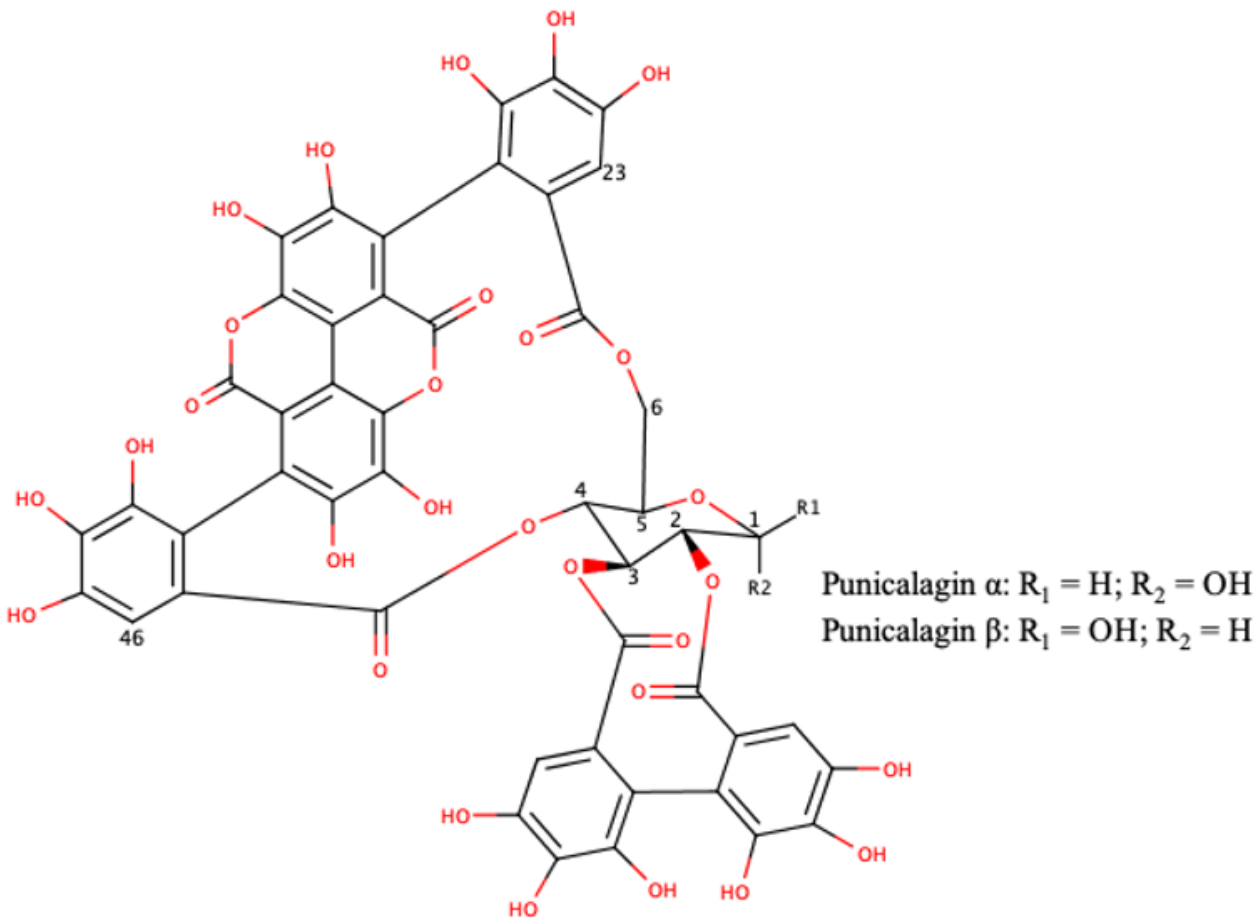

Figure 1

The chemical structures of α and β anomers of Punicalagin.

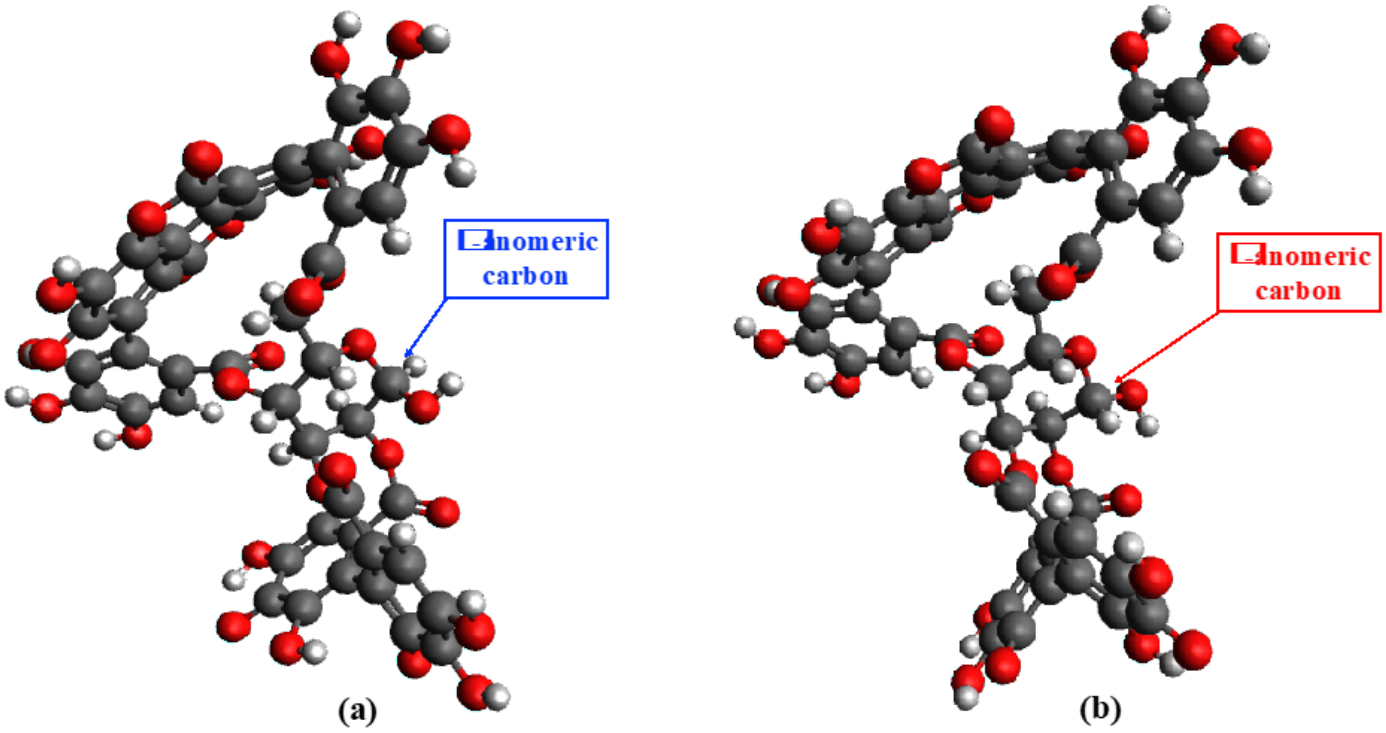

Figure 2

Optimized geometries of α (a) and β (b) anomers by using B3LYP/6-31+G(d,p) level of theory.

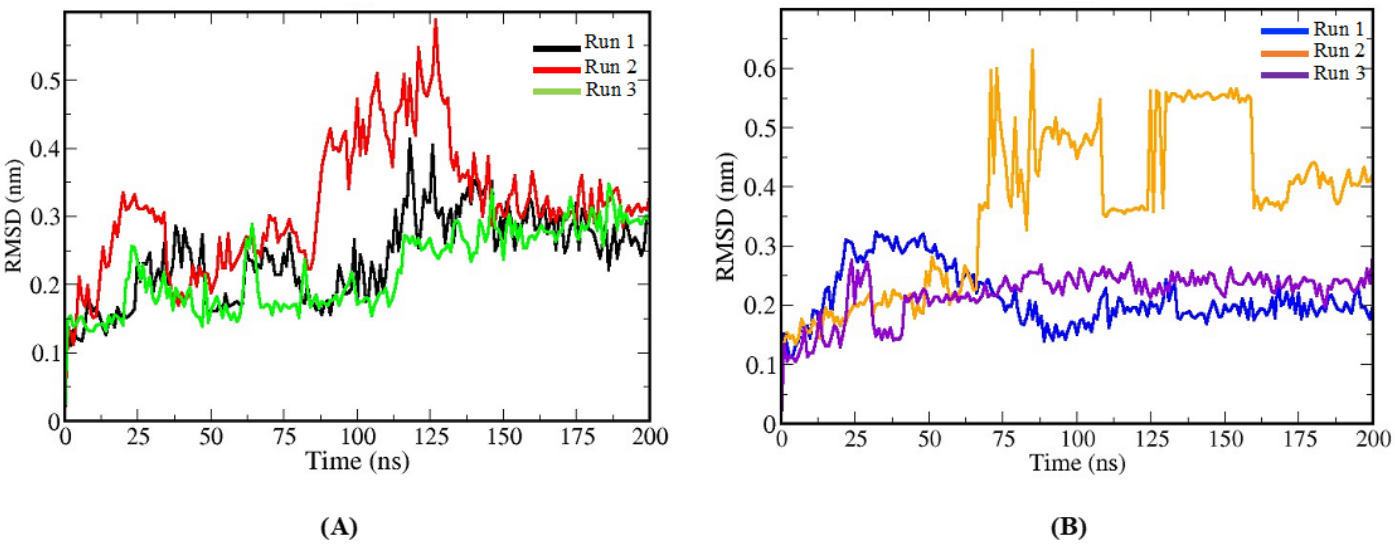

Figure 3

Root Mean Square Deviations (RMSD) for punicalagin α (A, black, red and green lines) and β (B, blue, orange and violet lines) anomers. All MD simulations were performed in three replicates each anomer studied.

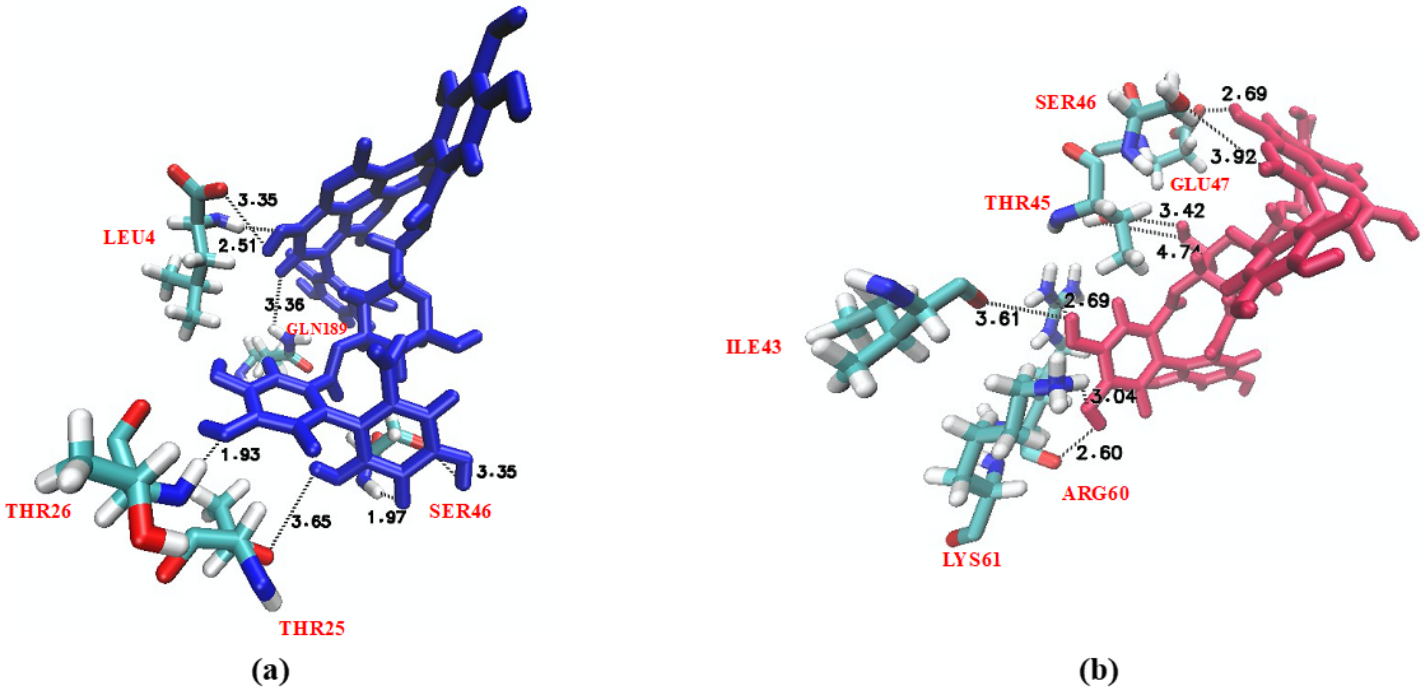

Figure 4

Details of interactions of α- (a) and β- (b) anomers with Mpro receptor residues. Black dashed lines represent hydrogen bonds between α- (a) or β- (b) anomer with pocket Mpro residues.

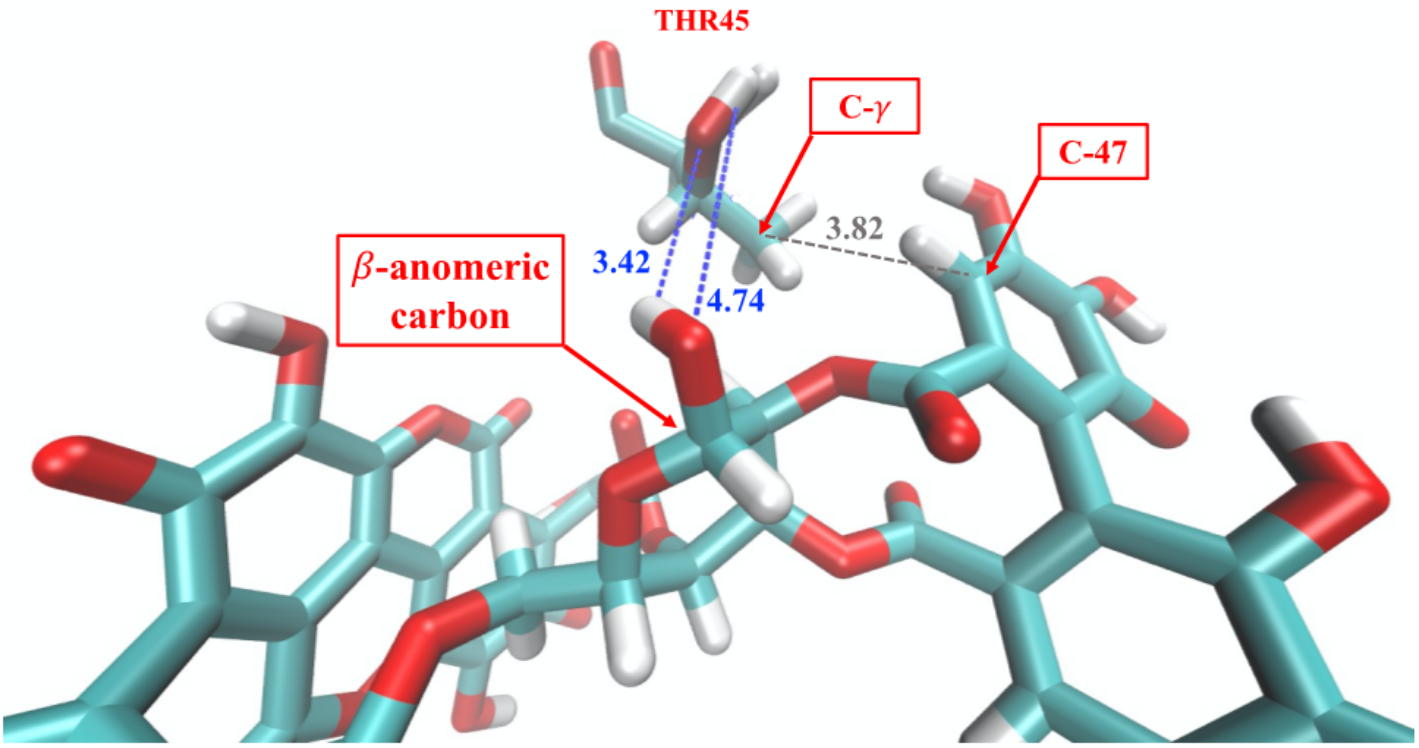

Figure 5

Representative highlight of non-covalent interactions between residue THR45 Mpro and β-anomer. The blue dashed lines are the hydrogen bonds and gray dashed line is the hydrophobic interaction.

Supplementary Files

This is a list of supplementary files associated with this preprint. Click to download.

- Supplementarymaterialfigurestables.pdf